

Article

Two-Photon Lifetime Imaging of Voltage Indicating Proteins as a Probe of Absolute Membrane Voltage

Daan Brinks,¹ Aaron J. Klein,¹ and Adam E. Cohen^{1,2,3,*}¹Department of Chemistry and Chemical Biology, ²Department of Physics, and ³Howard Hughes Medical Institute, Harvard University, Cambridge, Massachusetts

ABSTRACT Genetically encoded voltage indicators (GEVIs) can report cellular electrophysiology with high resolution in space and time. Two-photon (2P) fluorescence has been explored as a means to image voltage in tissue. Here, we used the 2P electronic excited-state lifetime to probe absolute membrane voltage in a manner that is insensitive to the protein expression level, illumination intensity, or photon detection efficiency. First, we tested several GEVIs for 2P brightness, response speed, and voltage sensitivity. ASAP1 and a previously described citrine-Arch electrochromic Förster resonance energy transfer sensor (dubbed CAESR) showed the best characteristics. We then characterized the voltage-dependent lifetime of ASAP1, CAESR, and ArcLight under voltage-clamp conditions. ASAP1 and CAESR showed voltage-dependent lifetimes, whereas ArcLight did not. These results establish 2P fluorescence lifetime imaging as a viable means of measuring absolute membrane voltage. We discuss the prospects and improvements necessary for applications in tissue.

INTRODUCTION

Neuroscientists have long sought a robust tool for optical imaging of membrane voltage *in vivo* (1–4). With such a tool, one could probe synaptic weights by observing sub-threshold potentials in postsynaptic cells. One could also infer rules governing circuit-level function from high time-resolution maps of spiking activity in many cells. The key to achieving this goal is a good optical readout of voltage.

Thanks to recent advances in optogenetics, investigators have made significant progress toward achieving this goal. Genetically encoded voltage indicators (GEVIs) based on ArcLight (5,6), ASAP1 (7), rhodopsin derivatives (8–10), VSFP Butterfly (11), and electrochromic Förster resonance energy transfer (eFRET) (12,13) scaffolds show adequate combinations of sensitivity and speed to report action potentials in cultured neurons. Near-infrared, archaerhodopsin-derived QuasAr constructs can be paired with a blue-shifted channelrhodopsin to enable all-optical electrophysiology *in vitro* and in superficial cells in brain slices (8).

Optical recordings of neuronal activity *in vivo* have primarily relied on genetically encoded Ca²⁺ indicators. In small and transparent organisms such as the zebrafish (14) and *C. elegans* (15,16), optical sectioning is often performed by means of one-photon (1P) techniques, including light-sheet (14), structured illumination (17), confocal (16), and light-field (18) microscopies. Simultaneous voltage and Ca²⁺ imaging was recently demonstrated in the zebrafish heart, but the measurements obtained relied on the period-

icity of the heartbeat for signal averaging (19). For larger brains that are highly scattering, two-photon (2P) approaches are preferred. In comparison with 1P excitation, 2P excitation provides better depth penetration, lower background autofluorescence, and less tissue damage (1,20,21). Recently, 2P Ca²⁺ imaging via GCaMP3 or GCaMP6 was paired with optical stimulation of a red-shifted channelrhodopsin (22,23) for all-optical interrogation of circuit function *in vivo*. 2P voltage imaging with organic voltage-sensitive dyes has been practiced for several years (1,2). 2P voltage imaging was recently combined with simultaneous 2P calcium imaging (24), and small 2P signals were obtained *in vivo* with the GEVI VSFP-Butterfly 1.2 (11).

Most fluorescence voltage measurements report relative changes in voltage. Accurately calibrated, or absolute, measurements of membrane voltage are confounded by variations in expression level, background autofluorescence, and signal decay by photobleaching, as well as instrument-specific variations in illumination intensity and collection efficiency. Two-wavelength ratiometric measurements help somewhat, but still require accurately calibrated illumination sources and are hindered by differential rates of photobleaching between the reporter and the reference. We previously explored the possibility of encoding absolute membrane voltage into the millisecond-timescale nonequilibrium dynamics of a rhodopsin photocycle (25), but this measurement required a complex multi-wavelength optical setup.

2P fluorescence offers the prospect of monitoring absolute voltage through the effect of voltage on electronic excited-state lifetime. The delay between absorption of the pulsed excitation photons and re-emission of the

Submitted April 2, 2015, and accepted for publication July 28, 2015.

*Correspondence: cohen@chemistry.harvard.edu

Editor: Hagan Bayley.

© 2015 by the Biophysical Society
0006-3495/15/09/0914/8

<http://dx.doi.org/10.1016/j.bpj.2015.07.038>



fluorescence photon depends only on the electronic structure of the fluorophore and its interactions with its local environment, including voltage. Lifetime is thus insensitive to the sources of variation that confound measurements of intensity. If voltage affects the lifetime, 2P fluorescence lifetime imaging (2P-FLIM) could provide a readout of the absolute voltage. 1P- and 2P-FLIM are routinely used for quantitative measurements, often in combination with genetically encoded sensors based on FRET (21,26–29). To our knowledge, this technique has not previously been applied to measure absolute membrane voltage.

To benchmark the field and to determine the most promising directions for future efforts, we compared the 2P photophysical and voltage-sensing attributes of the most widely used GEVIs and tested them for absolute voltage reporting.

MATERIALS AND METHODS

Microscopy and electrophysiology

For a detailed description of the materials and methods used in this work, see [Supporting Materials and Methods](#) in the [Supporting Material](#). Briefly, we built an inverted beam-scanning 2P fluorescence microscope optimized for excitation at wavelengths between 950 and 1300 nm, and for detection of fluorescence at wavelengths shorter than 775 nm (Fig. 1 A). Illumination was provided by a pulsed, 120 fs laser, tunable between 680 and 1300 nm at an 80 MHz repetition rate. Fluorescence was detected on a photomultiplier tube (PMT) in photon-counting mode. Single photoelectron pulses were digitized and detected using a computer-controlled data acquisition system. Simultaneously, fluorescence lifetime measurements were performed with the use of a time-correlated single-photon-counting (TCSPC) unit.

We coupled a patch-clamp amplifier to the setup to obtain electrophysiological and optical measurements simultaneously. The electrophysiology and optical measurements were synchronized via custom software written in LabView and MATLAB (The MathWorks, Natick, MA).

Cell culture

Experiments were performed in HEK293T cells and in cultured rat hippocampal neurons. HEK cells were grown and transfected according to standard protocols (8,30). P0 hippocampal neurons were cultured in neurobasal-based medium on preestablished glial monolayers as described previously (8,31–33) and transfected according to the calcium phosphate transfection protocol (34). All animal experiments were approved by the Harvard Institutional Animal Care and Use Committee.

RESULTS

2P voltage imaging

We acquired 2P fluorescence images of HEK cells expressing ASAP1 and simultaneously varied the membrane voltage via a patch pipette (Fig. 1 B; [Movie S1](#)). In initial experiments, we used raster-scan imaging of a rectangular field of view. Fluorescence values were integrated over each frame. At a 6 Hz frame rate, the voltage-equivalent fluorescence noise was 10 mV for a cell expressing ASAP1.

Several factors conspire to limit the time resolution of 2P voltage imaging. To acquire adequate photon counts, one must be able to ensure sufficient integration time at the signal-generating pixels. At faster frame rates, photon shot noise degrades the signal/noise ratio (SNR). Increasing the

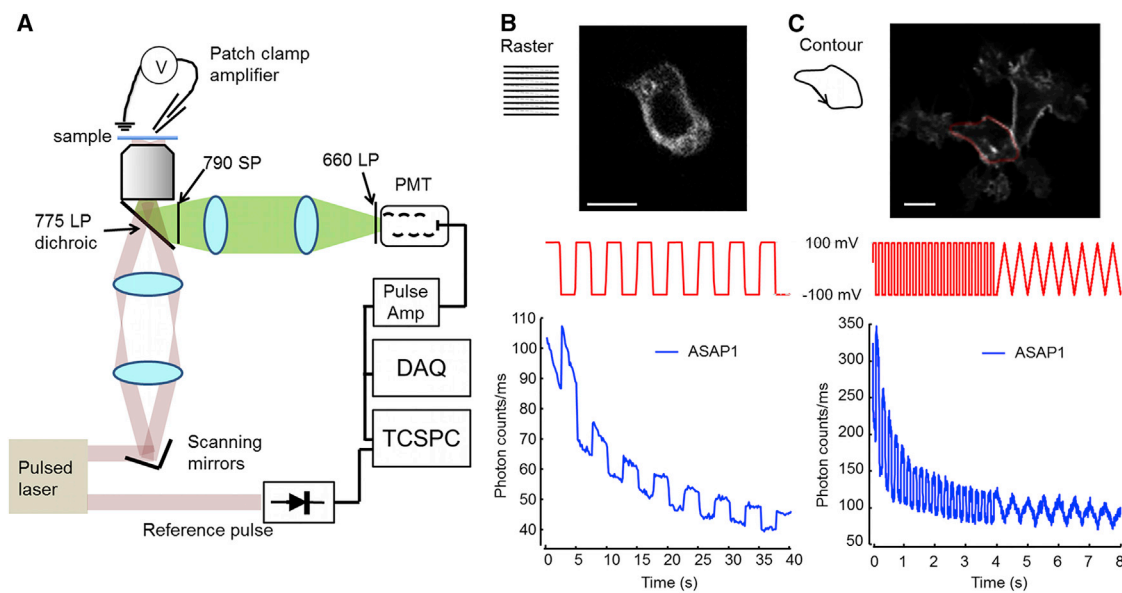


FIGURE 1 Voltage imaging with 2P fluorescence. (A) A beam-scanning 2P microscope. Laser pulses with a duration of ~ 120 fs and tunable wavelength between 950 and 1300 nm were directed into the back aperture of a 60×1.2 NA water immersion objective via scanning mirrors. Fluorescence at wavelengths shorter than 775 nm was detected by imaging the objective back aperture onto a PMT in a cooled housing. (B) Top: single frame from a movie acquired in raster-scan mode of a HEK cell expressing ASAP1 ([Movie S1](#)). Middle: applied membrane voltage, 0.2 Hz step function. Bottom: raw whole-frame fluorescence, sampled at 6 Hz. (C) Top: image of a HEK cell expressing ASAP1, with the contour scan superimposed in red ([Movie S2](#)). Middle: applied membrane voltage, 5 Hz step function, 1 Hz ramp function. Bottom: raw fluorescence integrated over the contour, sampled at 500 Hz. Scale bars, 10 μm . To see this figure in color, go online.

illumination intensity helps with shot noise but leads to increased photodamage and photobleaching. As a practical matter, frame rates can also be limited by either maximum galvo acceleration or maximum laser power.

Raster scanning is inefficient for voltage imaging because the laser spot spends most of its time either outside or inside the cell, while voltage-dependent fluorescence comes predominantly from the cell membrane (Fig. S1). For a cell with a diameter of 10 μm , imaged in an equatorial plane with a pixel size of 600 nm diameter, the ratio of the number of voltage-insensitive intracellular pixels to voltage-sensitive membrane pixels is $\sim 330:1$. Thus, one can achieve a large gain in signal by keeping the laser on the cell membrane.

To minimize photobleaching, the measurement should be distributed over as many reporter molecules as possible. Thus, it is better to scan the laser around the membrane than to park it at a single spot. Similar principles are well established in the context of 2P optogenetic stimulation, with resonant scanners most commonly tracing a line, spiral, or circle (23,35), or acousto-optic deflectors tracing an arbitrary pattern (36). To maximize the amount of membrane protein interrogated, we adopted a contour-scanning approach (Fig. 1 C; Movie S2). The galvos were programmed to trace a cell membrane at a 500 Hz repetition rate. In a HEK cell expressing ASAP1, fluorescence traces reported membrane voltage with a voltage-equivalent noise of 17 mV in a 2 ms integration bin on a single-trial basis, which is a far better performance than was achieved in the raster-scan mode.

Signal-generating pixels are illuminated with a higher duty cycle in contour-scan mode than in raster-scan mode. Thus, the increased time resolution of contour-scan mode comes at the cost of an increased photobleaching rate. In raster-scan mode the photobleaching lifetime (time to 50% of initial intensity) of ASAP1 was $t_{\text{bleach}} = 30$ s, whereas in contour-scan mode the photobleaching lifetime was $t_{\text{bleach}} = 1$ s. For a fixed laser intensity, the photobleaching rate is inversely proportional to the number of diffraction-limited spots in the scan. In raster-scan mode there were $\sim 2.5 \times 10^4$ spots in the image, whereas in contour-scan mode there were only ~ 100 spots in the contour.

Probe comparison: intensimetric voltage imaging

We compared the 2P voltage-sensing properties of several GEVIs: ArcLight A242 (5), QuasAr1-mOrange (8), QuasAr2-eGFP (8), ASAP1 (7), and a citrine-QuasAr2 eFRET construct that we dubbed citrine-Arch eFRET sensor (CAESR) (12) (Fig. 2; Table 1).

In each case, the cell was first imaged via raster scanning. For the QuasAr constructs, cells expressing protein were identified by imaging the bright fluorescent protein linked to the QuasAr (Fig. S3). The fluorescence of the plasma membrane was then recorded under contour scanning along

a manually defined path around the cell. Fig. 2 shows the average fluorescence responses for steps in membrane voltage between ± 100 mV. The sensitivities and response times of the reporters are given in Table 1. ASAP1 and QuasAr2 showed the best combination of voltage sensitivity and response speed, so these reporters were subjected to ramps in membrane voltage to evaluate their linearity (Fig. 2).

The apparent brightness of a reporter is sensitive to many experimental details, including the expression level, illumination intensity, choice of emission filters, and spectral response of the detector. Fig. 2 K and Table 1 show the brightness values measured in our setup. Each measurement was performed with a time-average excitation power of ~ 4 mW.

Photobleaching is sensitive in a nonlinear manner to details of illumination conditions that are likely to differ between setups. Furthermore, most of the sensors did not show simple single-exponential decays. The method we used to estimate photostability is described in Supporting Materials and Methods. ASAP1 started out 50-fold brighter than QuasAr2, but ASAP1 photobleached 25-fold faster to half its starting brightness (Fig. S4).

The mOrange-QuasAr2 eFRET probe showed voltage-sensitive fluorescence under 1P, but not 2P, illumination (Fig. S5). In contrast, 2P illumination of CAESR at 968 nm led to a gradual increase in voltage-sensitive fluorescence (Fig. S6). These observations illustrate that the 1P and 2P behaviors of GEVIs can be dramatically different, likely due to the complex photophysics of microbial rhodopsins. One should exercise caution in extrapolating from one measurement modality to the other.

2P imaging of action potentials

Expression levels, protein folding, and membrane trafficking can differ between neurons and HEK cells. Therefore, we expressed the two best-performing GEVIs, ASAP1 and QuasAr2, in neurons to test the possibility of detecting 2P action potentials.

We imaged neurons via wide-field single-photon epifluorescence to find cells with good protein expression (Fig. 3 A), and used differential interference contrast (DIC) to assess the health of the cell membrane (Fig. 3 A). Highly expressing and healthy neurons were then imaged in 2P excitation (Fig. 3 A). Using whole-cell current-clamp electrophysiology, we injected current pulses to induce action potentials. Simultaneously, we scanned the laser focus along the membrane in contour-scan mode and recorded the resulting 2P fluorescence. Action potentials were not detectable with QuasAr2. ASAP1 reported action potentials at the single-trial level with an SNR of 1. Averaging three temporally registered action potentials made the AP clearly resolvable in the photon trace (Fig. 3 B). From the marginal SNR in vitro, we deemed the ASAP1 signal unlikely to be

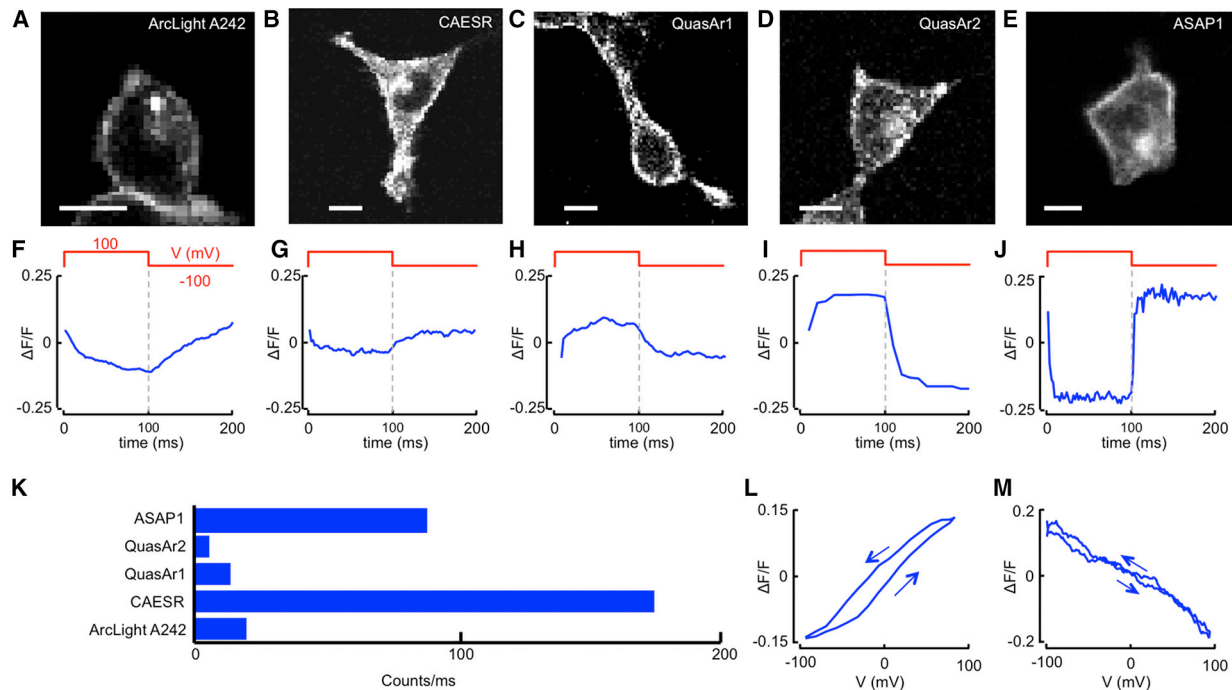


FIGURE 2 Comparison of GEVIs for 2P voltage detection. (A–E) Raster-scanned 2P images of HEK cells expressing (A) ArcLight A242, (B) CAESR, (C) QuasAr1, (D) QuasAr2, and (E) ASAP1. For ArcLight, CAESR, and ASAP1, the image is of the fluorescence of the probe itself, excited with the wavelength that is also used for the voltage-sensitive measurements. For the QuasAr constructs, the image is of a bright fluorescent protein (QuasAr1: mOrange $\lambda_{exc} = 1080$ nm, QuasAr2: eGFP, $\lambda_{exc} = 950$ nm) fused to the QuasAr construct to facilitate cell selection. Scale bars, 10 μm . (F–J) $\Delta F/F$ in 2P excitation of (F) ArcLight A242, (G) CAESR, (H) QuasAr1, (I) QuasAr2, and (J) ASAP1. (K) Comparison of brightness between the tested GEVIs. (L and M) Fluorescence as a function of membrane voltage for (L) QuasAr2 and (M) ASAP1, recorded for voltages increasing and decreasing with time. The fluorescence shows some hysteresis depending on the direction of the voltage sweep. To see this figure in color, go online.

robustly useful in vivo for detecting neuronal action potentials. Modest improvements in the brightness or voltage sensitivity of this construct could change that assessment.

Lifetime

The ability of a GEVI to report voltage through the excited-state lifetime depends on the physical mechanism of voltage

sensing. Voltage can affect fluorescence by acting in either the ground state (e.g., by changing the ground-state absorption spectrum) or the electronic excited state (e.g., by changing the branching ratio between fluorescence and nonradiative decay). In the former scenario, voltage will not affect lifetime, whereas in the latter it will.

When voltage affects the rate of nonradiative decay, the excited-state lifetime is

TABLE 1 Photophysical Properties of Common GEVIs for 2P Voltage Imaging

Construct	λ_{exc} (nm)	λ_{em} (nm)	$\Delta F/F$ per 100 mV ^a	Brightness (counts/ms) ^b	Fractional Shot Noise in 1 ms ^c	Response Time (ms) ^d	t_{bleach} (s) ^e
ArcLight A242	950	<775	0.08	20	0.2	50 (100)	50
CAESR	968	<775	0.03	175	0.08	5 (5)	3
QuasAr1	1200	660–775	0.04 ± 0.01 ($n = 8$)	13 ± 10	0.3	2* (0.05)	25
QuasAr2	1200	660–775	0.08 ± 0.02 ($n = 5$)	6 ± 3	0.4	10* (1)	25
ASAP1	950	<775	0.23 ± 0.03 ($n = 6$)	80 ± 40	0.1	2* (1)	1

^aVoltage sensitivity, $\Delta F/F$ per 100 mV, was calculated by normalizing to the average of $F(100 \text{ mV})$ and $F(-100 \text{ mV})$ (Figs. 2 and S2).

^bBrightness depends on many experimental details and was determined from the average photon counts in a user-defined region of interest comprising the membrane of a highly expressing cell that was healthy enough to sustain a whole-cell patch-clamp recording.

^cShot noise calculated from $1/\sqrt{\text{counts/ms}}$. The shot-noise limit determines the value of $\Delta F/F$ that can be detected in a 1 ms interval with an SNR of 1.

^dResponse time (10–90%) of sensors to steps in voltage from -100 to 100 mV. Numbers in parentheses represent 1P literature values (12). Precise numerical agreement is not expected because the literature values were measured for steps between different voltages. In cases marked by an asterisk, the 2P response time was faster than the integration time, and the number given here is the integration time.

^ePhotobleaching lifetimes are specific to the experimental conditions, so only relative values are meaningful. Photobleaching rates are further influenced by multiexponential decay, nonlinear dependence on excitation power, and ultrafast pulse-induced photophysics. The values given are for the experiments plotted in Fig. 2.

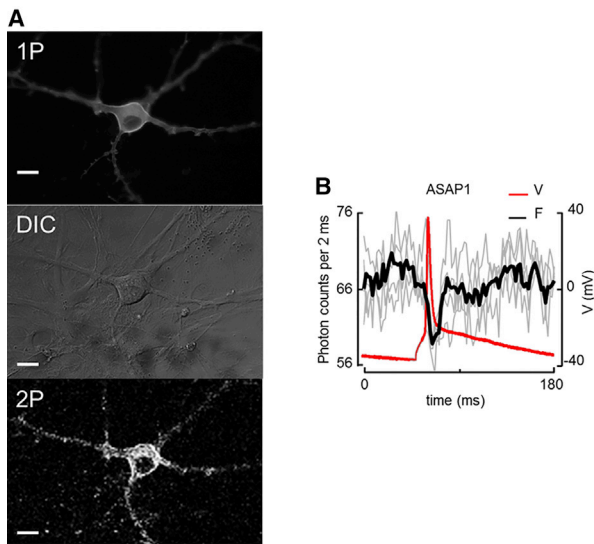


FIGURE 3 Detecting neuronal action potentials with 2P excitation. (A) Top: rat hippocampal neuron expressing ASAP1, imaged in 1P fluorescence to assess the protein expression level. Middle: cell imaged in DIC to assess cell health. The culture dish was then transferred to the 2P microscope. Bottom: cell imaged in 2P fluorescence. (B) 2P fluorescence versus time during action potentials elicited by current injection from a patch pipette. The perimeter of the soma was imaged in contour-scan mode and the fluorescence was recorded at 500 Hz. Red, voltage recording; gray, individual fluorescence recordings with an SNR of 1; black, average of three consecutive optical recordings. To see this figure in color, go online.

$$\tau_{es} = \frac{1}{k_{fl} + k_{nr}(V)},$$

where k_{fl} is the fluorescence emission rate and $k_{nr}(V)$ is the nonradiative decay rate. The fluorescence quantum yield (QY), proportional to steady-state fluorescence, is

$$QY = \frac{k_{fl}}{k_{fl} + k_{nr}(V)}.$$

Thus, in the case of voltage-dependent excited-state dynamics, one would expect the steady-state fluorescence and excited-state lifetime to have the same functional dependence on voltage. From steady-state fluorescence alone, one cannot determine a priori whether a GEVI will show a voltage-dependent excited-state lifetime.

We used TCSPC to probe the electronic excited-state lifetime. This measurement is independent of the number of probe molecules that are still active. Due to the severity of photobleaching in 2P measurements, lifetime is an attractive alternative to intensity measurements.

We constructed a TCSPC system to measure the delay between the excitation pulse and the emitted photons (Fig. 4 A). Briefly, a reference pulse synchronized with the laser excitation is detected by a fast photodiode. A photon emitted by the probe is detected on a PMT operated in single-photon Geiger mode. A fast start-stop timer re-

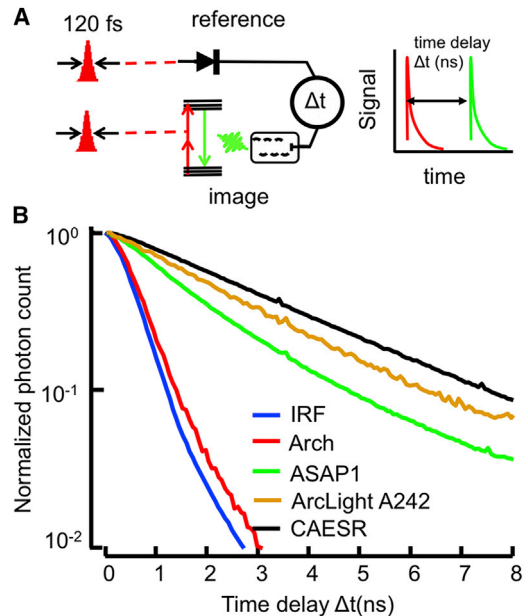


FIGURE 4 Apparatus for measuring 2P fluorescence lifetime. (A) Lifetime is detected via TCSPC. Two synchronized femtosecond pulses are emitted by the laser: one is detected on a fast photodiode and the other excites a fluorescent protein whose emission is detected on a PMT. The difference in arrival time between the reference and fluorescence is the lifetime for this excitation. (B) Histograms of the arrival times can be fitted to obtain the mean excited-state lifetime. The instrument response function is 600 ps.

records the time delay between these two events. A histogram of these time delays gives a distribution (Fig. 4 B) that can be fitted to an exponential decay to obtain the excited-state lifetime.

Probe comparison: absolute voltage detection through lifetime imaging

The excited-state lifetime of QuasAr2 was shorter than the instrument response function of 0.6 ns, and thus could not be accurately measured (Fig. 4 B). The lifetimes of the other probes were observable and distinguishable. At a membrane voltage of 0 V, the lifetimes of ASAP1, ArcLight A242, and CAESR were 1.8 ns, 2.5 ns, and 2.7 ns, respectively. These values are not corrected for the instrument response time.

We measured the voltage-dependent lifetimes of ArcLight A242, ASAP1, and CAESR. We anticipated that CAESR would have a voltage-dependent lifetime due to its hypothesized mechanism of action (a voltage-dependent change in the rhodopsin absorption spectrum leads to voltage-dependent nonradiative quenching of the citrine fluorescence (12)). For the other two constructs, we did not know what to expect.

We expressed the constructs in HEK cells and used whole-cell voltage clamp to apply the voltage trace shown in Fig. 5 A (top) while simultaneously monitoring the

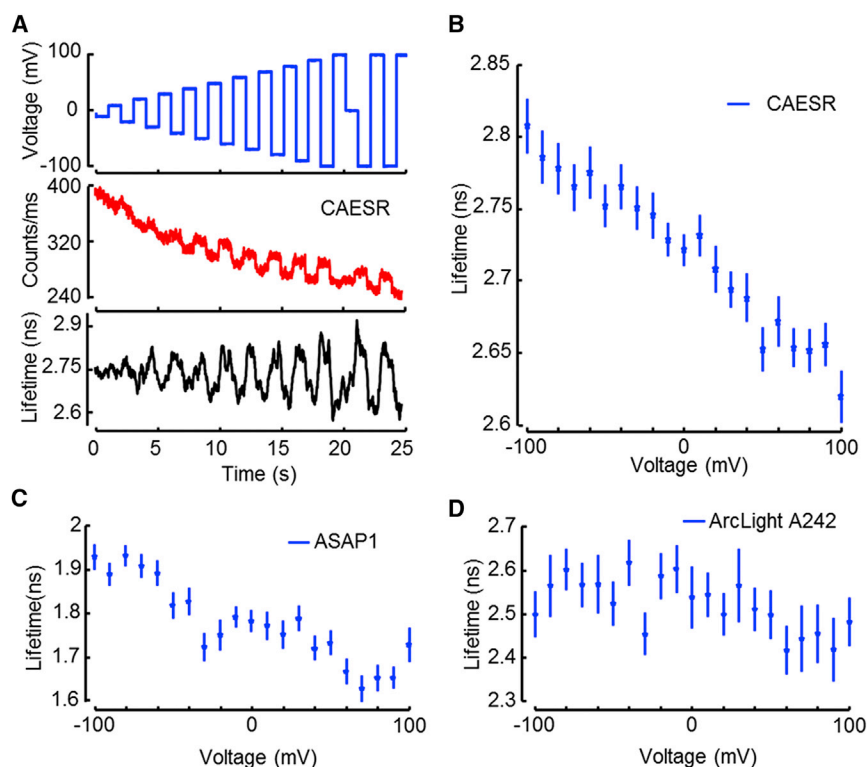


FIGURE 5 The 2P fluorescence lifetime encodes the absolute voltage. (A) Membrane voltage of a HEK cell expressing CAESR was modulated in 1 s intervals. The fluorescence intensity varied with voltage on top of a rapidly bleaching baseline. The fluorescence lifetime reports changes in voltage without drift in the average value. (B) The lifetime of CAESR can be calibrated to an absolute value of membrane voltage and reported voltage with a sensitivity of $\Delta\tau = -0.09$ ns per 100 mV. The noise-equivalent voltage was 20 mV in a 1 s bandwidth. (C) The ASAP1 fluorescence lifetime reported absolute voltage with a sensitivity of $\Delta\tau = -0.14$ ns per 100 mV, but saturated toward the edges. The noise-equivalent voltage was 30 mV in a 1 s bandwidth. (D) The fluorescence lifetime of ArcLight A242 did not show a discernible dependence on voltage. To see this figure in color, go online.

fluorescence and excited-state lifetime. The steady-state fluorescence of CAESR reported the voltage steps superimposed on a photobleaching baseline (Fig. 5 A, middle). The lifetime of CAESR was insensitive to photobleaching, illustrating the potential use of lifetime for absolute voltage measurements (Fig. 5 A, bottom).

The fluorescence lifetime of CAESR reported voltage with good linearity and a sensitivity of $\Delta\tau = -0.09$ ns per 100 mV (Fig. 5 B) between ± 100 mV. ASAP1 also showed a voltage-dependent lifetime, with $\Delta\tau = -0.14$ ns per 100 mV (Fig. 5 C) between ± 70 mV, but saturated at the extremes. The lifetime of ArcLight A242 (Fig. 5 D) did not show a detectable dependence on membrane voltage. These observations imply that in ASAP1, voltage acts in the electronic excited state, but in ArcLight A242, it acts in the electronic ground state. A recently introduced voltage-sensitive dye, VF2.1.Cl (37), also showed a voltage-dependent 2P excited-state lifetime, with $\tau(0 \text{ mV}) = 3.16$ ns and $\Delta\tau = 0.11$ ns per 100 mV, consistent with the proposed mechanism of voltage-dependent quenching of the electronic excited state.

In lifetime measurements with CAESR, the voltage-equivalent noise was 20 mV in a 1 s bandwidth. Thus, a brighter or more sensitive reporter is needed for high-time-resolution measurements, e.g., of neuronal or cardiac action potentials. Existing reporters offer adequate sensitivity to measure resting potential or slow modulatory changes. We propose the name 2P absolute contrast lifetime image voltage sensing (2PAC LIVS) for this technique.

DISCUSSION

2P voltage imaging offers the possibility of recording electrical activity in tissue, as well as measuring absolute membrane voltage via its effect on the excited-state lifetime. However, at present, both applications have limited sensitivity and are confounded by photobleaching. The sensitivity of 2PAC LIVS is only 20 mV in a 1 s bandwidth. Thus, this technique might be appropriate for measuring slow variations in resting voltage, but it is not appropriate for measuring fast dynamics. Here, we consider the prospects for improving both the molecular reporters and the instrumentation.

2P voltage imaging places severe demands on the brightness and photostability of the molecular reporters. Fig. 6 compares the signal sources for Ca^{2+} imaging and voltage imaging, in both 1P and 2P imaging modalities. 2P voltage imaging acquires signal from ~ 100 -fold fewer molecules and requires an ~ 100 -fold higher time resolution compared with 2P Ca^{2+} imaging (Supporting Materials and Methods). Thus, to achieve a similar SNR, 2P voltage imaging requires an excitation rate per molecule, Γ , that is $\sim 10^4$ -fold higher than that required for 2P Ca^{2+} imaging. Photobleaching rates grow as Γ^α , with the exponent $\alpha \geq 1$ (38,39). Thus, even if the brightness, signal amplitude, and photostability were similar between the voltage and Ca^{2+} reporters, achieving 2P voltage imaging with the same SNR as 2P Ca^{2+} imaging would lead to an $\sim 10^4$ -fold faster photobleaching rate.

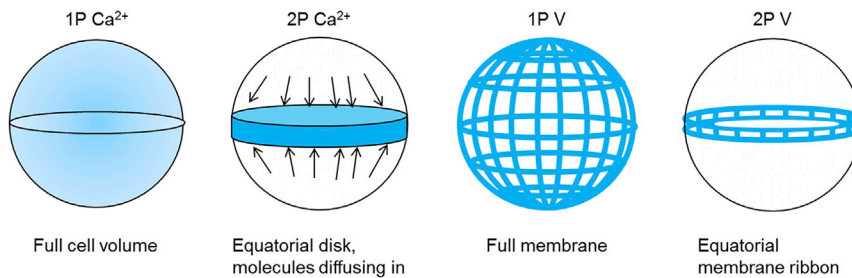


FIGURE 6 Comparison of the number and location of probes that contributed to calcium and voltage detection in 1P and 2P excitation. For a given signal rate (photons/s), the rate of photobleaching is inversely proportional to the number of reporter molecules that contribute to this signal. In 1P epifluorescence Ca²⁺ imaging, the signal comes from the 3D bulk of the cell. In 2P Ca²⁺ imaging, the signal comes from molecules within a single focal plane. However, relatively fast cytoplasmic diffusion replenishes photobleached molecules, leading to an effective sampling volume

close to the 3D bulk. In 1P epifluorescence voltage imaging, voltage-dependent signals can come from the whole-cell membrane. In 2P voltage imaging, only molecules at the equator contribute signal. Diffusion of GEVIs in the lipid membrane is too slow to replace photobleached molecules on an experimentally relevant timescale. For equal count rates of signal-bearing photons, 2P voltage imaging will experience a higher photobleaching rate than 2P Ca²⁺ imaging. To see this figure in color, go online.

Considering the limited scope for improvements in the photostability and brightness of GFP-based reporters, we conclude that progress toward achieving 2P voltage imaging with these probes must rely on improvements in voltage sensitivity and speed. For example, the response time of ASAP1 leads to modest low-pass filtering of neuronal action potentials. An increased speed of response would enhance the ASAP1 signal for action potential detection. Another route would be to develop probes with scaffolds that are not based on GFP or its homologs. QuasAr2, for instance, has sufficient photostability and sensitivity, but is not bright enough for 2P detection of neuronal action potentials.

Improvements in optics could facilitate 2P voltage imaging by enabling near-simultaneous sampling of a larger portion of the cell membrane. To increase the number of molecules that contribute to the signal, one should increase the area of the membrane that contributes. A simple strategy may be to decrease the numerical aperture of the excitation beam, thereby increasing the Rayleigh length and the length of the 2P excitation spot. Around the cellular equator, a longer spot would sample molecules at a greater range of latitudes. The attendant increase in beam width would necessitate an increase in laser power.

In principle, one could further decrease the photobleaching rate while maintaining the signal by scanning the laser in a 3D trajectory over the cell membrane. This approach is technically challenging because one must first map the cell surface with high resolution and then scan rapidly while simultaneously rapidly modulating the focal plane. However, rapid 3D scanning 2P systems have been developed to address this issue (36,40).

Neither the molecular nor the instrumentation routes toward 2P voltage imaging or FLIM are exceedingly promising, particularly if one seeks to apply these techniques in tissue or in vivo. Practical voltage imaging in tissue will likely require alternative imaging schemes such as light-sheet or 1P structured illumination (41–43), photoacoustic or photothermal imaging (44,45), and light-gated voltage integrators (46).

CONCLUSIONS

We have shown the potential of 2P detection of membrane voltage in two modalities: detection of relative changes in the fluorescence intensity and detection of absolute voltage in the fluorescence lifetime. Although the 2P fluorescence brightness of the current generation of GEVIs is too low to allow recordings of single-trial action potentials, measurements obtained with a slower time resolution are feasible. Detection of the fluorescence lifetime provides a measure of absolute voltage that is not biased by photobleaching.

SUPPORTING MATERIAL

Supporting Materials and Methods, Supporting Discussion, six figures, and two movies are available at [http://www.biophysj.org/biophysj/supplemental/S0006-3495\(15\)00773-0](http://www.biophysj.org/biophysj/supplemental/S0006-3495(15)00773-0).

AUTHOR CONTRIBUTIONS

D.B. and A.E.C. designed research. D.B. performed research. D.B. and A.E.C. wrote the manuscript. All of the authors contributed analytic tools and analyzed data.

ACKNOWLEDGMENTS

We thank Guiping Wang, Hohjai Lee, Vaibhav Joshi, and Katherine Williams for technical assistance. We also thank Peng Zou for the CAESR plasmid, Michael Z. Lin for ASAP1, Vincent Pieribone for ArcLight, and Evan Miller for samples of VF2.1.Cl.

This work was supported by a Presidential Early Career Award for Scientists and Engineers (N00014-11-1-0549), National Institutes of Health grants R01EB012498-02 and DP2OD007428, the Gordon and Betty Moore Foundation, and the Howard Hughes Medical Institute. D.B. received a Rubicon grant from the Netherlands Organization for Scientific Research.

REFERENCES

1. Fisher, J. A., J. R. Barchi, ..., B. M. Salzberg. 2008. Two-photon excitation of potentiometric probes enables optical recording of action

- potentials from mammalian nerve terminals in situ. *J. Neurophysiol.* 99:1545–1553.
2. Acker, C. D., P. Yan, and L. M. Loew. 2011. Single-voxel recording of voltage transients in dendritic spines. *Biophys. J.* 101:L11–L13.
 3. Cohen, L. B., B. M. Salzberg, ..., C. H. Wang. 1974. Changes in axon fluorescence during activity: molecular probes of membrane potential. *J. Membr. Biol.* 19:1–36.
 4. Salzberg, B. M., A. Grinvald, ..., W. N. Ross. 1977. Optical recording of neuronal activity in an invertebrate central nervous system: simultaneous monitoring of several neurons. *J. Neurophysiol.* 40:1281–1291.
 5. Jin, L., Z. Han, ..., V. A. Pieribone. 2012. Single action potentials and subthreshold electrical events imaged in neurons with a fluorescent protein voltage probe. *Neuron.* 75:779–785.
 6. Piao, H. H., D. Rajakumar, ..., B. J. Baker. 2015. Combinatorial mutagenesis of the voltage-sensing domain enables the optical resolution of action potentials firing at 60 Hz by a genetically encoded fluorescent sensor of membrane potential. *J. Neurosci.* 35:372–385.
 7. St-Pierre, F., J. D. Marshall, ..., M. Z. Lin. 2014. High-fidelity optical reporting of neuronal electrical activity with an ultrafast fluorescent voltage sensor. *Nat. Neurosci.* 17:884–889.
 8. Hochbaum, D. R., Y. Zhao, ..., A. E. Cohen. 2014. All-optical electrophysiology in mammalian neurons using engineered microbial rhodopsins. *Nat. Methods.* 11:825–833.
 9. Flytzanis, N. C., C. N. Bedbrook, ..., V. Gradinaru. 2014. Archaelhodopsin variants with enhanced voltage-sensitive fluorescence in mammalian and *Caenorhabditis elegans* neurons. *Nat. Commun.* 5:4894.
 10. Gong, Y., J. Z. Li, and M. J. Schnitzer. 2013. Enhanced archaelhodopsin fluorescent protein voltage indicators. *PLoS One.* 8:e66959.
 11. Akemann, W., M. Sasaki, ..., T. Knöpfel. 2013. Two-photon voltage imaging using a genetically encoded voltage indicator. *Sci. Rep.* 3:2231.
 12. Zou, P., Y. Zhao, ..., A. E. Cohen. 2014. Bright and fast multicoloured voltage reporters via electrochromic FRET. *Nat. Commun.* 5:4625.
 13. Gong, Y., M. J. Wagner, ..., M. J. Schnitzer. 2014. Imaging neural spiking in brain tissue using FRET-opsin protein voltage sensors. *Nat. Commun.* 5:3674.
 14. Ahrens, M. B., M. B. Orger, ..., P. J. Keller. 2013. Whole-brain functional imaging at cellular resolution using light-sheet microscopy. *Nat. Methods.* 10:413–420.
 15. Guo, Z. V., A. C. Hart, and S. Ramanathan. 2009. Optical interrogation of neural circuits in *Caenorhabditis elegans*. *Nat. Methods.* 6:891–896.
 16. Leifer, A. M., C. Fang-Yen, ..., A. D. T. Samuel. 2011. Optogenetic manipulation of neural activity in freely moving *Caenorhabditis elegans*. *Nat. Methods.* 8:147–152.
 17. York, A. G., S. H. Parekh, ..., H. Shroff. 2012. Resolution doubling in live, multicellular organisms via multifocal structured illumination microscopy. *Nat. Methods.* 9:749–754.
 18. Prevedel, R., Y. G. Yoon, ..., A. Vaziri. 2014. Simultaneous whole-animal 3D imaging of neuronal activity using light-field microscopy. *Nat. Methods.* 11:727–730.
 19. Hou, J. H., J. M. Kralj, ..., A. E. Cohen. 2014. Simultaneous mapping of membrane voltage and calcium in zebrafish heart in vivo reveals chamber-specific developmental transitions in ionic currents. *Front. Physiol.* 5:344.
 20. Denk, W., J. H. Strickler, and W. W. Webb. 1990. Two-photon laser scanning fluorescence microscopy. *Science.* 248:73–76.
 21. Svoboda, K., and R. Yasuda. 2006. Principles of two-photon excitation microscopy and its applications to neuroscience. *Neuron.* 50:823–839.
 22. Rickgauer, J. P., K. Deisseroth, and D. W. Tank. 2014. Simultaneous cellular-resolution optical perturbation and imaging of place cell firing fields. *Nat. Neurosci.* 17:1816–1824.
 23. Packer, A. M., L. E. Russell, ..., M. Häusser. 2015. Simultaneous all-optical manipulation and recording of neural circuit activity with cellular resolution in vivo. *Nat. Methods.* 12:140–146.
 24. Crocini, C., R. Coppini, ..., L. Sacconi. 2014. Defects in T-tubular electrical activity underlie local alterations of calcium release in heart failure. *Proc. Natl. Acad. Sci. USA.* 111:15196–15201.
 25. Hou, J. H., V. Venkatachalam, and A. E. Cohen. 2014. Temporal dynamics of microbial rhodopsin fluorescence reports absolute membrane voltage. *Biophys. J.* 106:639–648.
 26. Yasuda, R., C. D. Harvey, ..., K. Svoboda. 2006. Supersensitive Ras activation in dendrites and spines revealed by two-photon fluorescence lifetime imaging. *Nat. Neurosci.* 9:283–291.
 27. Coda, S., A. J. Thompson, ..., C. Dunsby. 2014. Fluorescence lifetime spectroscopy of tissue autofluorescence in normal and diseased colon measured ex vivo using a fiber-optic probe. *Biomed. Opt. Express.* 5:515–538.
 28. Robinson, T., P. Valluri, ..., A. J. de Mello. 2014. Analysis of DNA binding and nucleotide flipping kinetics using two-color two-photon fluorescence lifetime imaging microscopy. *Anal. Chem.* 86:10732–10740.
 29. Ebrecht, R., C. Don Paul, and F. S. Wouters. 2014. Fluorescence lifetime imaging microscopy in the medical sciences. *Protoplasma.* 251:293–305.
 30. Kralj, J. M., A. D. Douglass, ..., A. E. Cohen. 2012. Optical recording of action potentials in mammalian neurons using a microbial rhodopsin. *Nat. Methods.* 9:90–95.
 31. McCarthy, K. D., and J. de Vellis. 1980. Preparation of separate astroglial and oligodendroglial cell cultures from rat cerebral tissue. *J. Cell Biol.* 85:890–902.
 32. Goslin, K. 1998. *Culturing Nerve Cells.* MIT Press, Cambridge, MA.
 33. Chen, G., N. C. Harata, and R. W. Tsien. 2004. Paired-pulse depression of unitary quantal amplitude at single hippocampal synapses. *Proc. Natl. Acad. Sci. USA.* 101:1063–1068.
 34. Jiang, M., and G. Chen. 2006. High Ca²⁺-phosphate transfection efficiency in low-density neuronal cultures. *Nat. Protoc.* 1:695–700.
 35. Rickgauer, J. P., and D. W. Tank. 2009. Two-photon excitation of channelrhodopsin-2 at saturation. *Proc. Natl. Acad. Sci. USA.* 106:15025–15030.
 36. Duemani Reddy, G., K. Kelleher, ..., P. Saggau. 2008. Three-dimensional random access multiphoton microscopy for functional imaging of neuronal activity. *Nat. Neurosci.* 11:713–720.
 37. Miller, E. W., J. Y. Lin, ..., R. Y. Tsien. 2012. Optically monitoring voltage in neurons by photo-induced electron transfer through molecular wires. *Proc. Natl. Acad. Sci. USA.* 109:2114–2119.
 38. Patterson, G. H., and D. W. Piston. 2000. Photobleaching in two-photon excitation microscopy. *Biophys. J.* 78:2159–2162.
 39. Chen, T. S., S. Q. Zeng, ..., W. Zhou. 2002. High-order photobleaching of green fluorescent protein inside live cells in two-photon excitation microscopy. *Biochem. Biophys. Res. Commun.* 291:1272–1275.
 40. Katona, G., G. Szalay, ..., B. Rózsa. 2012. Fast two-photon in vivo imaging with three-dimensional random-access scanning in large tissue volumes. *Nat. Methods.* 9:201–208.
 41. Voie, A. H., D. H. Burns, and F. A. Spelman. 1993. Orthogonal-plane fluorescence optical sectioning: three-dimensional imaging of macroscopic biological specimens. *J. Microsc.* 170:229–236.
 42. Mertz, J. 2011. Optical sectioning microscopy with planar or structured illumination. *Nat. Methods.* 8:811–819.
 43. Müller, C. B., and J. Enderlein. 2010. Image scanning microscopy. *Phys. Rev. Lett.* 104:198101.
 44. Wang, X., Y. Pang, ..., L. V. Wang. 2003. Noninvasive laser-induced photoacoustic tomography for structural and functional in vivo imaging of the brain. *Nat. Biotechnol.* 21:803–806.
 45. Boyer, D., P. Tamarat, ..., M. Orrit. 2002. Photothermal imaging of nanometer-sized metal particles among scatterers. *Science.* 297:1160–1163.
 46. Venkatachalam, V., D. Brinks, ..., A. E. Cohen. 2014. Flash memory: photochemical imprinting of neuronal action potentials onto a microbial rhodopsin. *J. Am. Chem. Soc.* 136:2529–2537.

Two-photon lifetime imaging of voltage indicating proteins as a probe of absolute membrane voltage

Daan Brinks¹, Aaron Klein¹, Adam E. Cohen^{1,2,3}

¹ Department of Chemistry and Chemical Biology, ² Department of Physics, Harvard University, Cambridge, MA 02138, USA, ³ Howard Hughes Medical Institute
cohen@chemistry.harvard.edu

Supplementary Information

Materials and Methods

Discussion of relative signal levels in 2P Ca²⁺ imaging vs voltage imaging

Movie Captions

Figures 1 – 6

Materials and Methods

Microscopy and electrophysiology

We built a beam-scanning two-photon microscope optimized for excitation at wavelengths between 950 and 1300 nm, and for detection of fluorescence at wavelengths shorter than 775 nm. Illumination was provided by a Spectra Physics Insight DeepSee, tunable between 680 and 1300 nm, with pulses of ~120 fs at 80 MHz repetition rate. The pulse dispersion was adjusted via an internal, motorized prism pair compressor controlled by Spectra Physics software.

The beam was steered onto the back aperture of an Olympus water immersion UPLANSAPO 60XW objective (NA 1.2) by a pair of galvo mirrors (Cambridge Technology 6215HM40B, driven by Cambridge Technologies 671215H-1HP Micromax servo driver on the X-axis and Cambridge Technologies 671215H-1 Micromax servo driver on the Y-axis). The imaging plane was selected by moving the objective with a Thorlabs MTS25-Z8 linear stage. Fluorescence emission was separated from back-scattered excitation light via a Semrock 775 nm long-pass dichroic beam splitter (FF775-Di01-25x36). Residual laser light was rejected using a Semrock 790 nm short-pass filter (FF01-790/SP-25). For the voltage sensitive measurements on QuasAr, an additional 664 nm long-pass filter (Semrock BLP01-664R-025) was added in the detection path to reject residual fluorescence of the appended bright fluorophore (mOrange or citrine).

Fluorescence was reimaged onto a Hamamatsu R943-02 PMT in photon counting mode. This PMT is optimized for sensitivity in the near infrared. To minimize dark-counts, the PMT was cooled to -20 °C using a Thermotek T252-P5B chiller. Single photon pulses were digitized using a Hamamatsu C9477 photon counting unit and counted with a National Instruments PCIe 6259 board.

A mirror on a motorized stage in the imaging path could be positioned to direct the image to an Andor Ixon X3 897 EMCCD for spatially resolved imaging of 1P or 2P signals. This pathway was also used in white light illumination when applying a patch pipette to a cell.

2P voltage imaging with GEVIs -- Supplement

We coupled a HEKA EPC 800 patch clamp amplifier to the setup to provide simultaneous electrophysiological and optical measurements. The pipette was positioned by a Sutter MP285 micromanipulator. Whole-cell voltage clamp and current clamp signals were filtered at 3 kHz with the internal Bessel filter and digitized with the same PCIe 6259 board. The electrophysiology and optical measurements were synchronized via custom software written in LabView.

In a typical experiment, cells were imaged in raster scan mode at a sampling rate of 4×10^5 pixels/s, in an area of $200 \times 200 \mu\text{m}^2$, at 256×256 pixel resolution, at a frame rate of 3.5 Hz. A bright and healthy cell was selected. The outline of a HEK cell was manually identified using custom LabView code. A patch pipette was then attached to the cell membrane and suction was applied to enter whole-cell mode following standard techniques. The membrane voltage was then varied while the laser was scanned rapidly along the membrane in a closed contour. The contour was sampled to 100 points. Fluorescence, current and voltage measurements on cells expressing ArcLight A242, CAESR or ASAP1 were recorded at 50 kHz sampling rate for a 500 Hz round-trip frequency; QuasAr1 was recorded at 40 kHz for a 400 Hz round-trip frequency; and QuasAr2 at 10 kHz for a 100 Hz round-trip frequency. The signal per round-trip is integrated and plotted as a function of time.

Dispersion in the high NA objective can undesirably broaden the excitation pulse, leading to a loss of peak intensity. We took care to minimize the pulse length in the focal plane for each excitation wavelength by maximizing the two-photon fluorescence of a test sample (Constellation Microspheres, Life Technologies) as a function of the position of the dispersion-compensating prisms.

We performed the contour scan experiment with an average laser power of 4 mW, for a time-average intensity at the laser focus of $2 \text{ MW}/\text{cm}^2$. For contour images containing 100 points, the time-average intensity at each spot in the contour was $20 \text{ kW}/\text{cm}^2$. Excitation intensities were calculated by measuring the mean power of the laser after the objective, divided by the diffraction-limited focal area ($\sim 500 \text{ nm}$ diameter).

Fluorescence lifetime

The secondary output beam of the Insight DeepSee laser was used to supply reference pulses for lifetime measurements. Pulses were detected using an ultrafast photodiode (Thorlabs Det10A). Single-photon pulses from the PMT were digitized (Hamamatsu C9477 photon counting unit), and then inverted using a Picoquant inverter. Reference and signal pulses were fed into a Time Correlated Single Photon Counter (TCSPC, Picoquant Picoharp 300H). Reference and signal pulses were synchronized by changing the length of coaxial cable between detector and TCSPC unit.

Each photon detection initiates a record of the “macro-time” and “micro-time.” The macro-time is the arrival time of the photon relative to the start of the experiment. The micro-time is the arrival time of the photon relative to the previous laser pulse. Binning and histogramming the macro-times supplies fluorescence intensity as a function of time;

2P voltage imaging with GEVIs -- Supplement

binning and histogramming the micro-times supplies a histogram that can be fitted to an exponential decay to obtain the fluorescence lifetime.

Fluorescence lifetime and electrophysiology data are synchronized by inserting into the photon record electronic markers at fixed points in the experiment. These markers are time-stamped and saved into the photon stream. Custom LabView code synchronized the markers with the rest of the experiment. We recorded a marker at the start of every round-trip of the contour scan.

Lifetime data in HEK cells was recorded in 1 s increments with the voltage held at values between ± 100 mV.

The mean values of fluorescence lifetime in Fig. 5b were obtained by binning photons for a measurement time $t = 1$ s. The error on this measurement is given by binning the lifetime in 20 ms bins and calculating the s.e.m.. The measurement precision is 20 mV in a 1 s bandwidth.

Genetic constructs

ArcLight A242, CAESR, mOrange-Quasar1 and eGFP-Quasar2 were cloned into the FCK backbone; expression was driven by the upstream CMV promoter. ASAP1 was in the pcDNA3.1/Puro-CAG backbone, with expression driven by the CAG promoter. Addgene locations: ArcLight A242 in PCS2+, #36857; CAESR, #59172; FCK-Quasar1-mOrange, #51629; ASAP1, #52519; Quasar2-eGFP in FCK not on Addgene.

HEK cell culture

HEK293T cells were cultured and transfected following standard protocols(1, 2). Briefly, HEK293T cells were grown at 37 °C, 5% CO₂, in DMEM supplemented with 10% FBS and penicillin-streptomycin. For ArcLight A242, Quasar and CAESR plasmids, 400 ng of plasmid DNA was transfected using Transit 293T (Mirus) following the manufacturer's instructions and assayed 48 h later. For ASAP1, 200 ng of plasmid DNA was transfected. The day before recording, cells were replated onto glass-bottom dishes (In Vitro Scientific) at a density of $1-2 \times 10^4$ cells/cm².

All imaging and electrophysiology were performed in Tyrode's medium (containing, in mM: 125 NaCl, 2.5 KCl, 3 CaCl₂, 1 MgCl₂, 10 HEPES, 30 glucose, pH 7.3, and adjusted to 305–310 mOsm with sucrose). A gap junction blocker, 2-aminoethoxydiphenyl borate (2-APB, 50 μ M, Sigma), was added to eliminate electrical coupling between cells.

Filamented glass capillaries (WPI, 1B150F-4, 1.5/0.84 mm OD/ID) were pulled to micropipettes (Sutter P-1000) with a tip resistance of < 5 M Ω and filled with internal solution containing 125 mM potassium gluconate, 8 mM NaCl, 0.6 mM MgCl₂, 0.1 mM CaCl₂, 1 mM EGTA, 10 mM HEPES, 4 mM Mg-ATP, 0.4 mM Na-GTP (pH 7.3), adjusted to 295 mOsm with sucrose. Pipettes were positioned with a Sutter MP285 micromanipulator.

Neuron culture

2P voltage imaging with GEVIs -- Supplement

All procedures involving animals were in accordance with the US National Institutes of Health Guide for the care and use of laboratory animals and were approved by the Institutional Animal Care and Use Committee at Harvard.

Rat glial monolayers were prepared as described previously (2, 3). Briefly, 10^6 dissociated hippocampal cells from P0 rat pups were plated on a 10-cm culture dish in glial medium, GM, composed of 15% FBS (Life), 0.4% (w/v) D-glucose, 1% GlutaMAX (Life), 1% penicillin/streptomycin (Life) in MEM (Life). When the dish reached confluence (1–2 weeks), cells were split using trypsin onto glass-bottom dishes (In Vitro Scientific, D35-20-1.5-N) coated with poly(D-lysine) and Matrigel (BD Biosciences) at a density of 3,500 cells/cm². After 3–6 days, glial monolayers were at or near confluence, and the medium was replaced by GM with 2 μ M cytarabine (cytosine- β -arabinofuranoside, Sigma) to prevent further glial growth. Dishes were maintained in GM with 2 μ M cytarabine until use. Dishes were discarded if microglia or neurons were identified on the monolayers.

Hippocampal neurons from P0 rat pups were dissected and cultured in neurobasal-based medium (NBAciv4, Brainbits) at a density of 30,000–40,000 neurons/cm² on the pre-established glial monolayers. At 1 day *in vitro* (DIV), cytarabine was added to the neuronal culture medium at a final concentration of 2 μ M to inhibit further glial growth (4).

Neurons were transfected between DIV 3 and DIV 8 via the calcium phosphate transfection method(5). Measurements on neurons were taken between DIV 7 and 18. Experiments were conducted in Tyrode's solution.

Data analysis

All error bars are s.e.m. unless stated otherwise. Measurements of voltage sensitivity ($\Delta F/F$) were acquired as follows. Membrane voltage was stepped in a square wave at 5 Hz, between ± 100 mV. To correct for photobleaching, a smoothed fluorescence trace was created using robust Loess method with a filter width of 200 ms. This smoothed trace showed no voltage-dependent fluorescence, only the photobleaching. The smoothed trace was subtracted from the raw fluorescence and the result was divided by the smoothed trace to yield a measure of $\Delta F/F$.

The data were then averaged over all cycles in the square wave ($n = 20$ for ASAP1, $n = 40$ for QuasAr1, QuasAr2 and CAESR, $n = 80$ for ArcLight A242). The triangle wave data were analyzed in a similar manner: $F_{\text{triangle}} = 2$ Hz, $n = 8$ repetitions for ASAP1, $n = 16$ for QuasAr2.

As an approximate measure of photostability, we determined the time for each reporter to bleach to 50% of its initial intensity. For the reporters where this value was reached within the time of measurement, it was read off directly. For reporters where this value was not reached within the measurement window, the final part of the trace was fitted to an exponential decay and the photobleaching time was determined via extrapolation.

The neuronal data were acquired in contour scan mode, sampling rate 50 KHz, round-trip frequency 500 Hz. Data were binned per round trip.

Lifetime data were acquired by binning photons with at 50 Hz sampling rate. We wrote custom code to obtain lifetimes from histograms of photon arrival times, allowing for simultaneous fitting of multiple histograms to speed up the fitting process. A global micro-time window was defined manually to avoid fitting to the part of the histogram dominated by our instrument response function. We fit the single-exponential decay to the function $A\exp(-t/\tau)+B$. The plot of lifetime vs time was smoothed using robust Loess method with a filter width of 300 ms.

The mean value for the lifetime was obtained by binning all photons obtained at a given voltage (measurement time 1 s) in one histogram and fitting an exponential decay; the error bars are s.e.m. based on the lifetime variations in 50 measurements sampled at 50 Hz.

Supplementary Discussion

Estimate of relative signal levels in 2P Ca²⁺ imaging vs voltage imaging

2P Ca²⁺ imaging excites molecules in a single plane transecting the cell body (Fig. 6). Diffusion in the cytoplasm rapidly replaces photobleached reporter molecules, so the effective reservoir of reporter molecules comprises the entire volume of the cell body. 2P voltage imaging excites molecules in an equatorial band in the plasma membrane. Due to slow diffusion in the plasma membrane, photobleached reporter molecules are not replenished.

Let us compare the number of Ca²⁺ reporters in the volume of a cell body to the number of voltage indicator molecules in the equatorial plane of the plasma membrane. We assume a linear spacing of 100 nm between molecules in both instances, a spherical cell body of 10 μm diameter, and a 2P imaging depth of 1 μm . The concentration of reporters in bulk is then 1.6 μM , and the number in the cell volume is approximately 5×10^5 . In a 1 μm wide equatorial band at the plasma membrane, the number of reporters is approximately 3×10^3 . Thus 2P voltage imaging relies on ~ 100 -fold fewer molecules than 2P Ca²⁺ imaging. While the underlying assumptions around geometry and expression levels may vary, the conclusion remains that vastly more molecules contribute in Ca²⁺ imaging than in 2P voltage imaging.

A further challenge for 2P voltage imaging is the requirement for higher time resolution: APs typically last 1-5 ms, while Ca²⁺ transients typically last 100-500 ms. Shorter exposure times require correspondingly higher illumination intensities to maintain comparable signal-to-noise ratios. Combining the geometrical effects and the increased need for time resolution implies that the photobleaching rate in 2P voltage imaging will be $\sim 10^4$ -fold higher than in Ca²⁺ imaging for recordings with comparable signal-to-noise ratio.

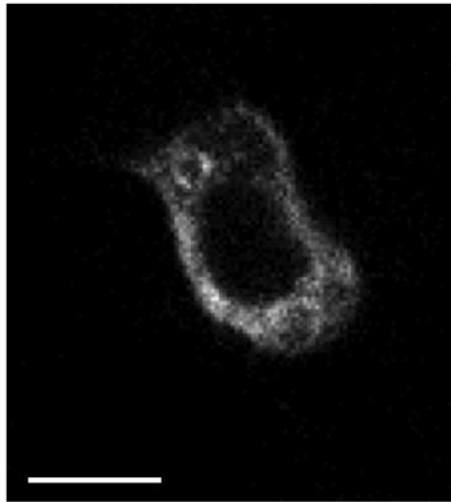
Supplementary Movies

Movie 1. Voltage imaging of ASAP1 via 2P fluorescence with raster-scan imaging. The membrane voltage was stepped according to the function depicted in Figure 1. Frames were recorded at 6 Hz.

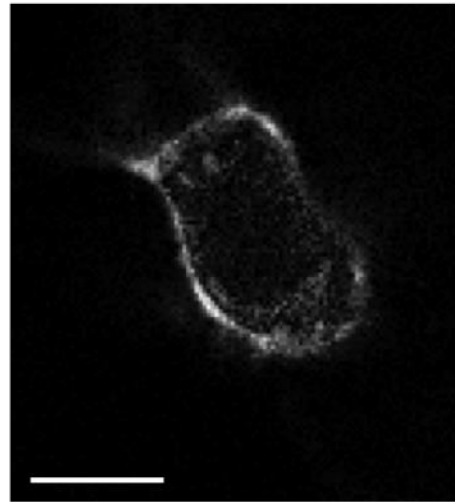
Movie 2. Voltage imaging of ASAP1 via 2P fluorescence with contour-scan imaging. The membrane voltage was modulated according to the function depicted in Figure 1. The time-dependent voltage signal is overlaid on a static raster-scan image of the cell. The first few cycles are omitted from the movie due to rapid initial photobleaching.

Supplementary Figures

A

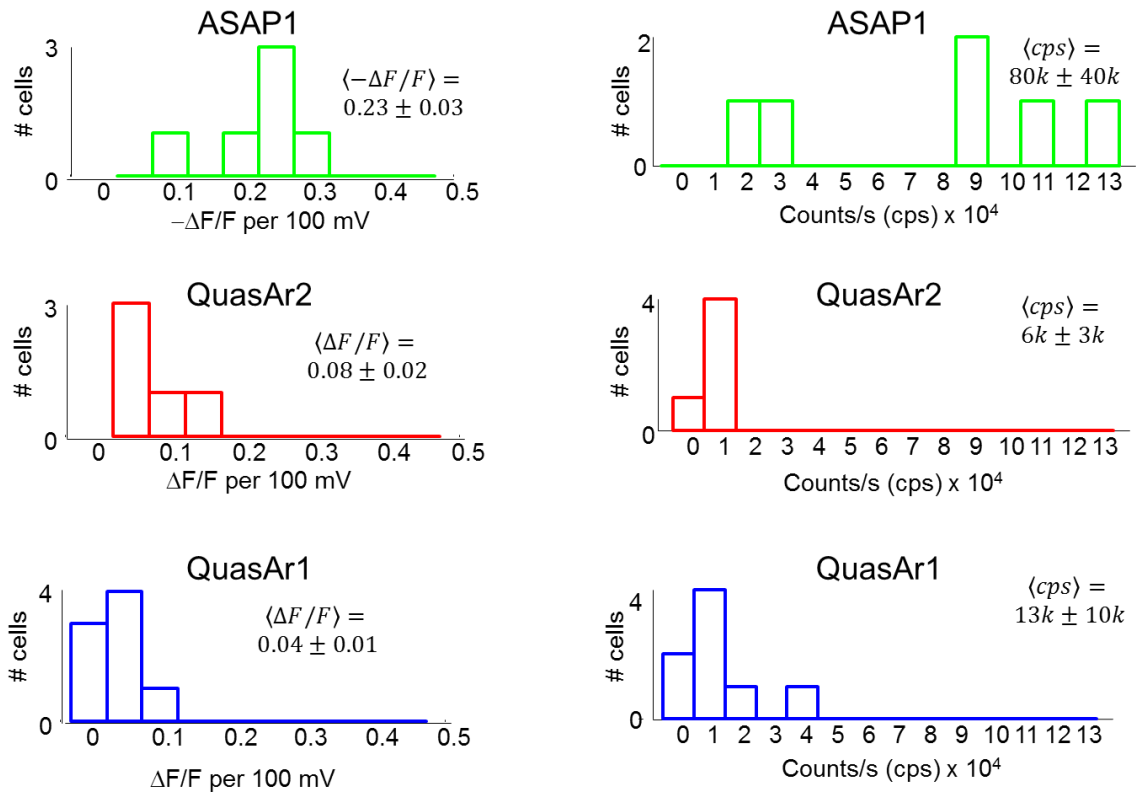


B

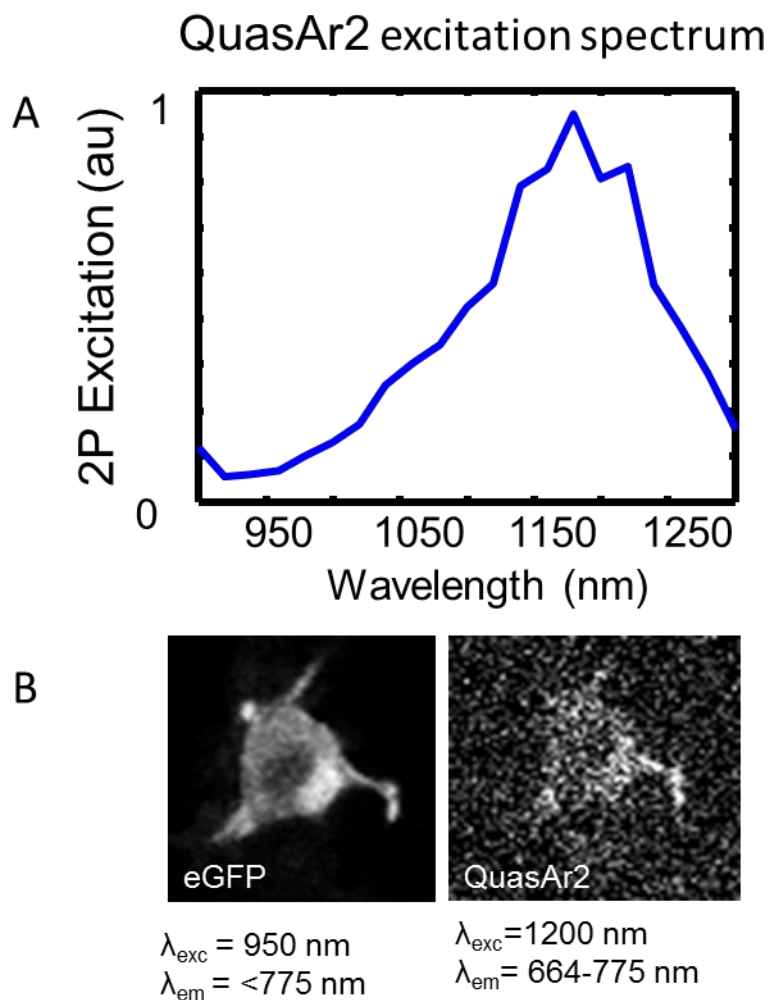


Supplementary figure 1. Voltage-sensitive pixels are predominantly in the cell membrane. (A) Image of a HEK cell expressing ASAP1, acquired via 2P fluorescence (same image as in Fig. 1B). (B) Cross-correlation of 2P fluorescence with membrane voltage, calculated at each pixel in the movie. Voltage-sensitive pixels are predominantly localized around the cell perimeter. Scale bars 10 μm .

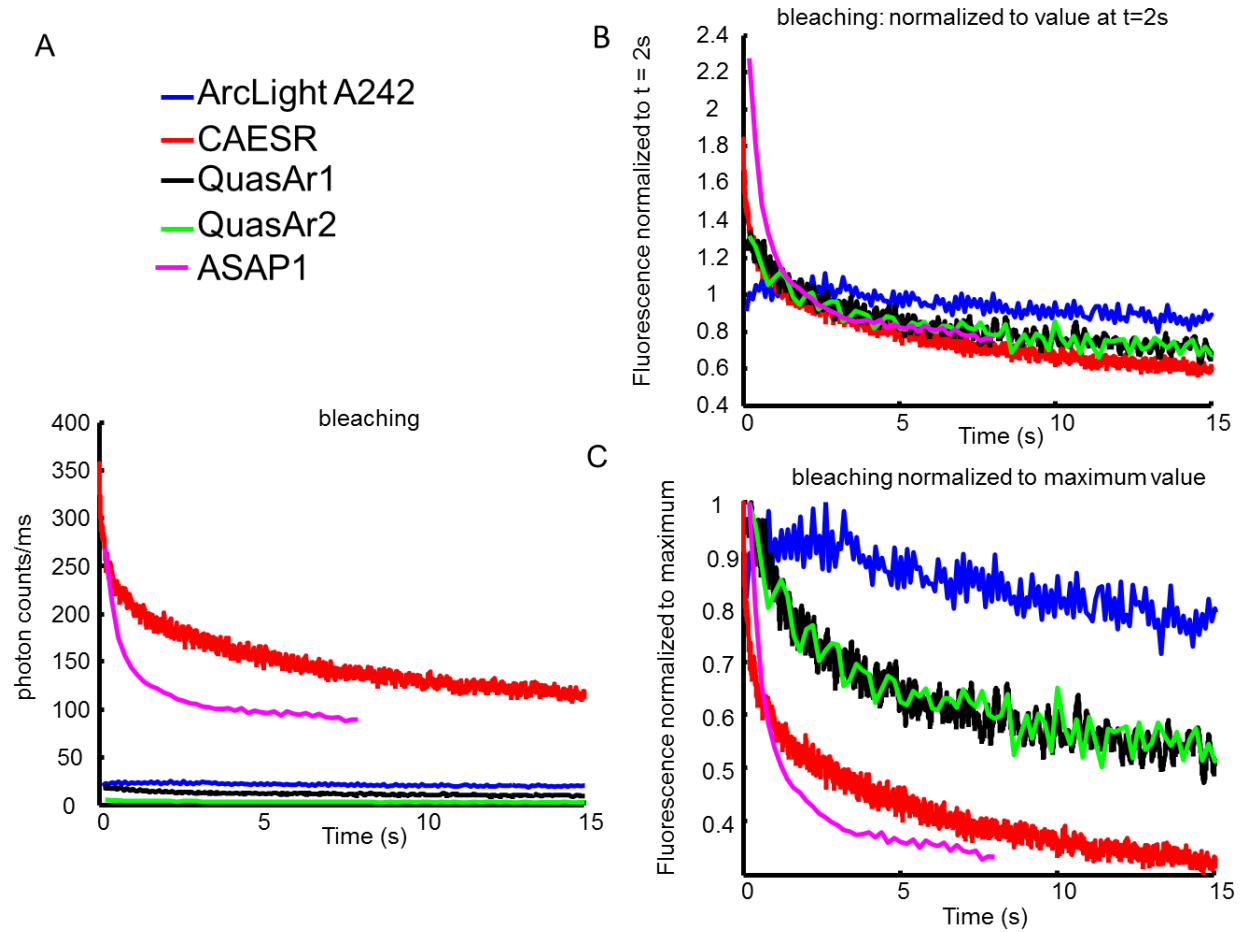
2P voltage imaging with GEVIs -- Supplement



Supplementary figure 2. Statistics of 2P voltage sensitivity and fluorescence brightness for ASAP1, QuasAr2, and QuasAr1 . Histograms represent measurements on $n = 5$ to 8 cells. The summary statistics represent population mean \pm s.e.m.

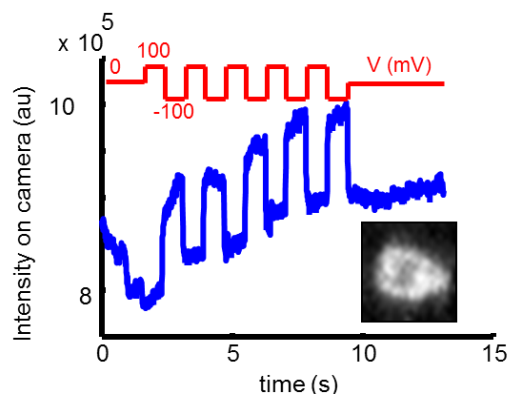


Supplementary figure 3. 2P excitation of QuasAr2. (A) Normalized 2P excitation spectrum of QuasAr2. 1200 nm excitation provided the best ratio between background autofluorescence and QuasAr2 fluorescence. (B) Comparison of 2P fluorescence from eGFP and QuasAr2 in a HEK cell expressing QuasAr2-eGFP. The signal-to-noise ratio of 2P-excited QuasAr2 fluorescence was not sufficient for fast raster scanning. The eGFP and QuasAr2 images were acquired with similar exposure times and laser powers.

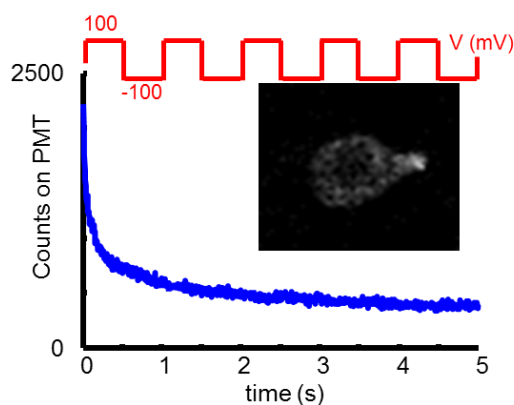


Supplementary figure 4. 2P photobleaching characteristics of GEVIs. (A) Raw recording. (B) Normalized to fluorescence at t=2 s. (C) Normalized to maximum fluorescence.

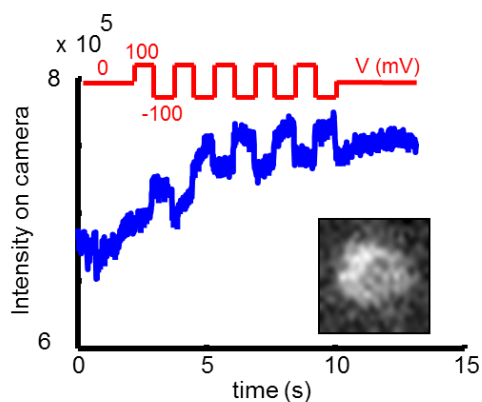
mOrange-QuasAr2 eFRET pair



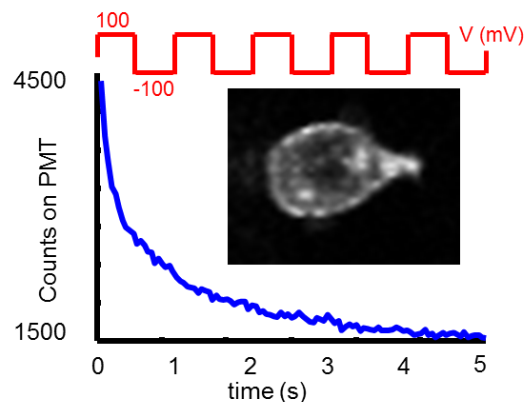
Measurement. 1: 532 nm 1P excitation, unsynchronized voltage steps



Measurement. 2: 1040 nm 2P excitation, synchronized voltage steps



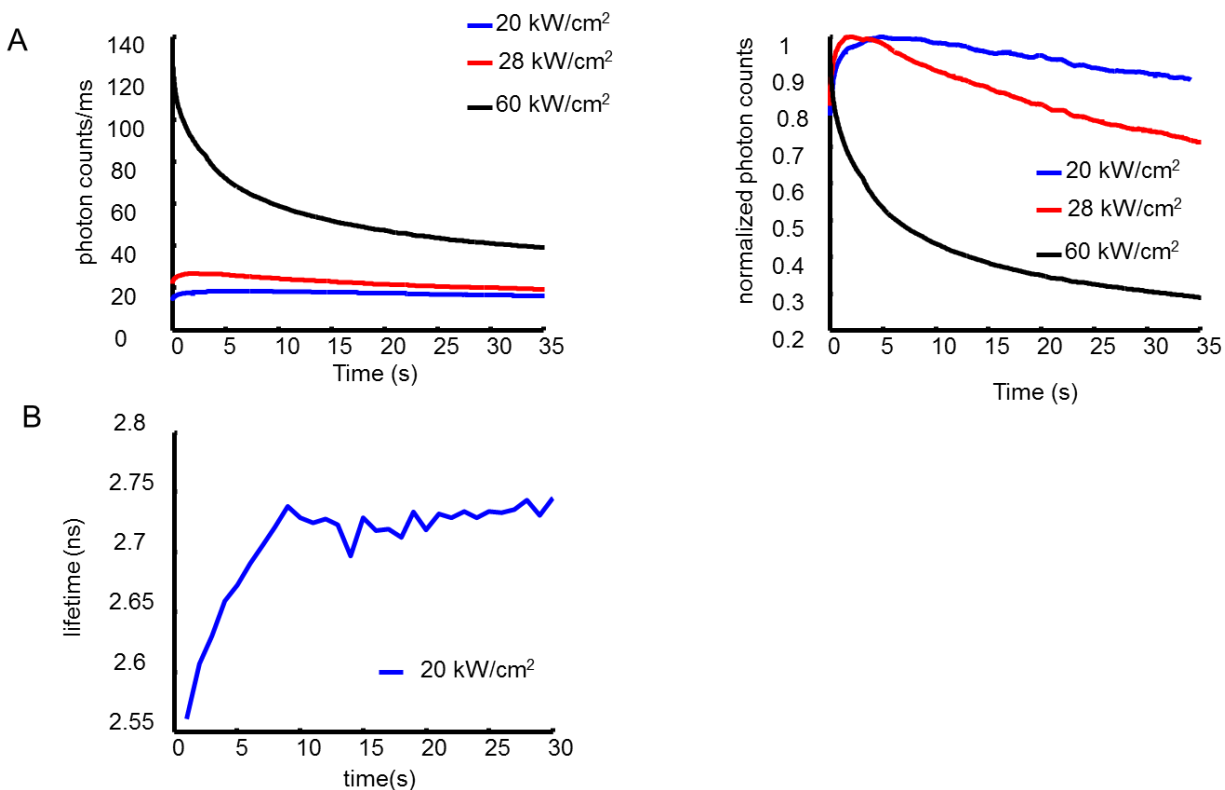
Measurement. 3: 532 nm 1P excitation, unsynchronized voltage steps



Measurement. 4: 1040 nm 2P excitation, synchronized voltage steps

Supplementary figure 5. Comparison between 1- and 2-photon excitation of an mOrange-QuasAr2 eFRET probe. Membrane voltage was stepped between ± 100 mV at 1 Hz in each measurement. Voltage-sensitive fluorescence was clearly observable in 1-photon fluorescence. The same cell was then imaged via 2-photon excitation. 2-photon fluorescence showed no dependence on membrane voltage. The cell was then imaged again with 1-photon excitation. The fluorescence regained sensitivity to voltage. A second switch to 2-photon excitation did not show dependence of fluorescence on voltage.

2P voltage imaging with GEVIs -- Supplement



Supplementary figure 6. 2-photon photoactivation of CAESR. (A). At low and moderate 2P excitation powers ($\lambda = 968$ nm) CAESR showed an initial gradual increase in citrine fluorescence, followed by a photobleaching decay. At higher excitation intensity the photoactivation behavior was masked by photobleaching. (B) The photoactivation also manifested as an increase in fluorescence lifetime.

Supporting References

1. Kralj, J. M., A.D. Douglass, D.R. Hochbaum, D. Maclaurin and A.E. Cohen. 2012. Optical recording of action potentials in mammalian neurons using a microbial rhodopsin. *Nat. Methods*. 9, 90-95.
2. Hochbaum, D. R., Y. Zhao, S. Farhi, N. Klapoetke, C.A. Werley, V. Kapoor, P. Zou, J.M. Kralj, D. Maclaurin, N. Smedemark-Margulies, J. Saulnier, G. Boulting, Y. Cho, M. Melkonian, G.K. Wong, D.J. Harrison, V.N. Murthy, B. Sabatini, E.S. Boyden, R.E. Campbell and A.E. Cohen. 2014. All-optical electrophysiology in mammalian neurons using engineered microbial rhodopsins. *Nat. Methods*. 11, 825-833.
3. McCarthy, K. D. and J. De Vellis. 1980. Preparation of separate astroglial and oligodendroglial cell cultures from rat cerebral tissue. *J. Cell Biol.* 85, 890-902.
4. Chen, G., N.C. Harata and R.W. Tsien. 2004. Paired-pulse depression of unitary quantal amplitude at single hippocampal synapses. *Proc. Nat. Acad. Sci. U. S. A.* 101, 1063-1068.
5. Jiang, M. and G. Chen. 2006. High Ca²⁺-phosphate transfection efficiency in low-density neuronal cultures. *Nature Protocols*. 1, 695-700.